DEUTSCHES ELEKTRONEN-SYNCHROTRON DESY

DESY 77/45
July 1977

QED Background to Heavy Lepton Production in e^+e^- Annihilation

by

F. Gutbrod and Z.J. Rek
Deutsches Elektronen-Synchrotron DESY, Hamburg

NOTKESTRASSE 85 · 2 HAMBURG 52

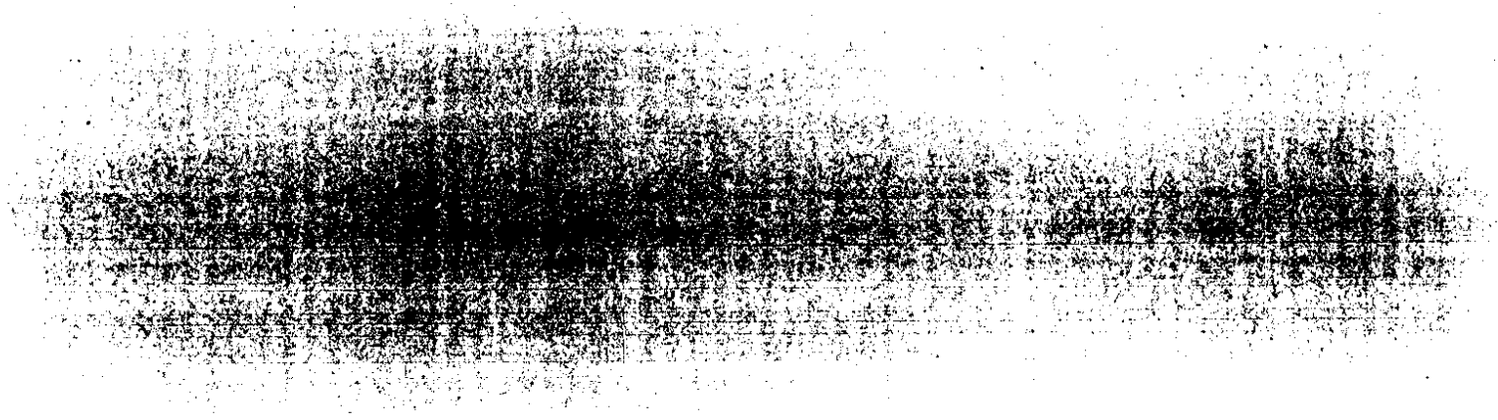

To be sure that your preprints are promptly included in the
HIGH ENERGY PHYSICS INDEX ,
send them to the following address (if possible by air mail) :

DESY
Bibliothek
Notkestraße 85
2 Hamburg 52
Germany

QED Background to Heavy Lepton Production in e^+e^- Annihilation

by

F. Gutbrod and Z.J. Rek [+)]

Deutsches Elektronen-Synchrotron DESY, Hamburg

Abstract

The contributions from two QED processes, $e^+e^- \to \mu^+\mu^-\gamma\gamma$ and $e^+e^- \to e^+e^-\mu^+\mu^-$, to the heavy lepton signal observed in muon inclusive final states in e^+e^- annihilation are calculated for the experimental setup of PLUTO in the energy range 4-5 GeV. Some modifications in the usual calculation techniques for QED processes are described. We discuss the observability of the sequential heavy lepton signal at PETRA energies and show which experimental cuts sufficiently damp the background to signal ratio.

[+)] On leave of absence from Institute of Nuclear Research, Warsaw, Poland.

1. Introduction

The inclusive muon cross section in e^+e^- annihilation certainly belongs to the experimentally cleanest and comparatively easily measurable channels for observing the recently discovered [1,2)] new heavy leptons via the reactions

$$e^+e^- \to \tau^+\tau^- \to e^\pm \mu^\mp + \text{neutrinos} \tag{1.1}$$

$$e^+e^- \to \tau^+\tau^- \to \mu^+\mu^- + \text{neutrinos} \tag{1.2}$$

$$e^+e^- \to \tau^+\tau^- \to \mu^\pm + \text{hadrons} + \text{neutrinos} \tag{1.3}$$

For these reactions there are 4 QED background processes, two of which ($e^+e^- \to \mu^+\mu^-$ and $e^+e^- \to \mu^+\mu^-\gamma$) are easily dealt with [2)] by an acoplanarity and a missing mass cut. The remaining two,

$$e^+e^- \to \mu^+\mu^-\gamma\gamma \tag{1.4}$$

and

$$e^+e^- \to e^+e^-\mu^+\mu^- \tag{1.5}$$

have to be calculated and integrated over the experimentally covered phase space. These calculations are difficult because i) they involve a seven dimensional integration with dramatically varying integrands, ii) the differential cross sections themselves are not trivial to obtain due to very large numerical cancellations, and iii) all experimental cuts have to be

incorporated in the integration limits. We therefore feel that calculations independent of those already existing [3,4] are worthwhile to present, especially if some technical progress can be achieved. Using as an example the cuts characteristic for the PLUTO experiment [2] we confirm the existing estimates [1,2] that the reactions (1.4) and (1.5) yield a background of the order of 10 % for the anomalous muon signal observed at SPEAR and DORIS which is attributed to the decay of a heavy lepton τ . Since the interpretation of the anomalous μ-signal depends strongly on the momentum spectra of the μ , we also calculate these and show that the corrections for them do not change the conclusions drawn in ref. (2).

Furthermore, in view of the pessimistic conclusions of ref. (4) concerning the observability of heavy leptons at PETRA/PEP energies because of the extremely copious production of muons in reaction (1.5), we propose some modifications of presently used experimental cuts which will clearly allow one to reduce the QED background to a small fraction of the heavy lepton signal at PETRA/PEP. In particular, the influence of the "energy scaled cuts" and of the detector acceptance is discussed quantitatively.

The paper is divided as follows. In section 2 which deals with reaction (1.4) we briefly discuss the construction of the differential cross section, then give the list of experimental cuts which can be converted into proper integration limits, such that modified Gaussian integration techniques can be applied. Especially the strong variation of the differential cross section with the photon angles relative to the electron directions is treated in an optimal way, resulting in very short computation times. The results for reaction (1.4) at $\sqrt{s}$ = 4-5 GeV are presented.

In section 3 we consider reaction (1.5). Special attention is given to a trick in the calculation of the matrix element which helps to get rid of enormous cancellations reported in the literature [3,4]. The results for the various charge combinations as a background to two-prong events and multiprong events are presented.

In section 4 we discuss both processes at $\sqrt{s}$ = 20 GeV and show that although the total cross section of (1.5) grows with s, whereas that of $e^+e^- \to \tau^+\tau^-$ decreases as 1/s, suitable cuts scaled with energy force (1.5) to fall as $\log s/s$ and make this reaction harmless as a background for two-prong events, at least for a detector with large angular acceptance ($\gtrsim$ 95 %).

Finally, in section 5 we list some conclusions and in the Appendix we give a more detailed description of our integration technique and the translation of experimental cuts into integration limits.

2. Reaction $e^+e^- \to \mu^+\mu^-\gamma\gamma$

2.1. Diagrams

Up to a permutation of the two photons there are three classes of diagrams depending on whether the photons are emitted from one or two different fermion lines. First of all, there are four "single radiation" diagrams with one photon emitted from each (electron and muon) line (fig. 1a-d). Then come three electron [+] "double radiation" diagrams (fig. 1e-g) and

[+] By "electron" we mean e^+ or e^-. If charges are important, we write them explicitly $e^{\pm}$.

finally three muon "double radiation" diagrams (fig. 1h-j).

The total number of diagrams is 20, due to the necessary interchange of the two photons. This amounts to 210 independent terms in the cross section.

2.2. Checks and Approximations

We have neglected the 3 muon double radiation diagrams, since the bulk of the cross section comes from the region where at least one photon is within a narrow cone around an electron, and the muon diagrams, fig. 1h-j, are not large there. This leaves us with 14 diagrams and 105 different interference terms and squares. They have been calculated and converted to FORTRAN subroutines by REDUCE [5]. The interference terms between the class of fig. 1a-d and that of fig. 1e-g are odd under $\mu^+\mu^-$-exchange, or, more precisely, $\sigma(b,j) \leftrightarrow -\sigma(a,j)$ and $\sigma(c,j) \leftrightarrow -\sigma(d,j)$ $(j = e,f,g)$ under the interchange of the muon four momenta. As an important check we have verified the interchange properties for all 105 terms. In most calculations we integrated symmetrically over μ^+ and μ^- coordinates and omitted the mentioned interference terms.

In order to check the overall normalization we have taken the diagrams of fig. 1a-d and compared the cross section integrated over photon directions, but with photon energies fixed and small, with the "soft photon formula" [6]

$$\frac{d\sigma}{d\Omega_\mu\, dE_{\gamma_1} dE_{\gamma_2}} \approx \frac{d\sigma^{\mu\mu}}{d\Omega_\mu} \frac{1}{E_{\gamma_1} E_{\gamma_2}} \left(\frac{2\alpha}{\pi}\right)^2 \left(\log \frac{4E_{e^+}^2}{m_e^2} - 1\right)\left(\log \frac{4E_{\mu^+}^2}{m_\mu^2} - 1\right) \qquad (2.1)$$

where $d\sigma^{\mu\mu}/d\Omega_\mu$ is the lowest order cross section for $e^+e^- \to \mu^+\mu^-$.

There is agreement within 15 % at $\sqrt{s}$ = 5 GeV, which is satisfactory in view of the large muon mass.

2.3. Experimental Cuts and Integration Method

Since the total cross section for background QED events is much larger than the heavy lepton signal, it has to be reduced by specific cuts. We shall list those applied in the PLUTO experiment [2], together with the cuts determined by the detector acceptance [+]. The apparatus-determined cuts are

a) $|\vec{p}_1| \geq p_{ex} = 1$ GeV — for the identified muon (outer detector), (2.2)

b) $|\vec{p}_2| \geq p_{min} = .25$ GeV — for the second particle (inner detector), (2.3)

c) $|\cos\vartheta_1| \leq \cos\vartheta_1^{min} = .75$ — required for good momentum resolution, (2.4)

d) $|\cos\vartheta_2| \leq \cos\vartheta_2^{min} = .87$ — as given by solenoid chambers. (2.5)

The QED-cuts are:

e) To get rid of the elastic $\mu^+\mu^-$ production, an acoplanarity cut is employed; $\phi_{12} > \phi_{AC} = 10^\circ$, or more precisely

$$|\mathrm{ang}\{(\vec{p}_1 \times \vec{p}_a), (\vec{p}_2 \times \vec{p}_a)\}| \leq \pi - \phi_{AC}. \qquad (2.6)$$

[+] We use the following notation: p_a, p_b = 4-momenta of the initial e^- and e^+ respectively; p_1 = 4-momentum of the muon identified as such in the outer detector, p_2 = that of the other charged particle (μ or e in reaction (1.5)) observed in the inner detector. The other 2 particles will have subscripts 3 and 4.

f) To reject $\mu^+\mu^-\gamma$ events, a large missing mass is required: if only particles 1 and 2 are detected,

$$(p_3 + p_4)^2 \geq MM = 1.4\,(\sqrt{s}\,/3.6\ \mathrm{GeV})^2. \qquad (2.7)$$

All these restrictions can be converted into explicit integration limits for the 2 muon three momenta (see Appendix). Now the last two cuts simplify the numerical integration of the differential cross section. First of all, the missing mass cut eliminates soft photons and the corresponding peak at zero photon energies. Secondly, the two photons cannot be emitted simultaneously in the beam direction, as this would lead to coplanar $\mu^+\mu^-$. Consequently, if we introduce as variables the two muon 3-momenta and the direction of one photon, the differential cross section is still strongly peaked in the photon angle with respect to the beam axis, but this type of peaking is that of ordinary bremsstrahlung, since the second photon must be at larger angles. Thus the typical singularity is known to be of the form

$$\frac{d\sigma}{d\vartheta_\gamma} = \frac{\sin\vartheta_\gamma}{(1 - \frac{v_e}{c}\cos\vartheta_\gamma)^2} \times \text{polynomial in } \sin^2\vartheta_\gamma. \qquad (2.8)$$

We have used the integration routine REGINA [7] to provide us with generalized Gaussian integration points for the weight function in (2.8). At $\sqrt{s}$ = 20 GeV 4 points in ϑ_γ were sufficient to reach an accuracy of better than 0.5 % for the ϑ_γ integral from 0 to 30 mrad. This method seems to be much superior to the logarithmic mapping technique [3], as the latter does not take care of the precise nature of the singularity at $\vartheta_\gamma = 0$.

For larger values of ϑ_γ it may happen that the second γ falls again into the narrow cone around the beam axis, which has been already integrated over. Thus there are complicated boundaries in the ϑ_γ integration for larger ϑ_γ, which are best handled by Monte Carlo techniques. The details are given in the Appendix.

2.4. Results

The total cross section for the observation of at least one of the muons in the outer and the second one in the inner detector independently of the photon variables is given as a function of $\sqrt{s}$ in Table 1. In this case the integration over energies and angles of the muons is fully symmetric. We found that the main contribution for all muon energies comes from the integration over photon angles in small cones around the initial electron and positron. With the cone angle of 8.6° this part amounts to 70 %. The similar cones around the muon directions give only 2 % contribution. The rest comes from the Monte Carlo calculation over the remaining solid angle of first photon (see Appendix).

The energy distribution $\frac{d\sigma}{dE_1}$ corresponds to the observation of one muon at the energy $E_1 (E_1 > 1\ \mathrm{GeV})$ in the outer detector and of the second muon in the outer or inner detector. This requires an asymmetric integration over energy, but due to the symmetry in ϑ the contribution from the interference terms vanishes. The curves representing $\frac{d\sigma}{dE_1}$ for the $\mu^+\mu^-\gamma\gamma$ process at 4 and 5 GeV are presented in the left part of Fig. 3 (short dashed curves).

The angular distribution $\frac{d\sigma}{d\cos\vartheta_1}$ of the muons may be defined in two ways:

1) Symmetric - corresponding to the charge averaged observation of one muon in the outer detector at the angle ϑ_1 with the second muon observed anywhere in the inner or outer detector. It is presented in fig. 4 (long dashed curve). Note that this distribution is more strongly peaked towards $\cos\vartheta_1 = 1$ than $1 + \cos^2\vartheta_1$.

2) Asymmetric, $d\sigma/d\cos\vartheta_{\mu^-}$, corresponding to the observation of $\mu^-(\mu^+)$ in outer detector under the angle ϑ_{μ^-} (ϑ_{μ^+}) with μ^+ (μ^-) observed anywhere in the inner or outer detector. The asymmetry comes from the contribution of interference terms. Both distributions $d\sigma/d\cos\vartheta_{\mu^-}$ and $d\sigma/d\cos\vartheta_{\mu^+}$ are drawn in fig. 4 (short dashed and dash-dotted curves respectively).

In fig. 5 we present the asymmetry

$$A(\vartheta) = \frac{d\sigma/d\cos\vartheta_{\mu^-} - d\sigma/d\cos\vartheta_{\mu^+}}{d\sigma/d\cos\vartheta_{\mu^-} + d\sigma/d\cos\vartheta_{\mu^+}} \qquad (2.8)$$

as a function of $\cos\vartheta$. Since the asymmetry is not small, it may be used as a test for the background in high statistics experiments.

3. The Process $e^+e^- \longrightarrow e^+e^-\mu^+\mu^-$

3.1. Diagrams, Approximations and Checks

Because of limited acceptance this process can fake a two prong event, especially if the differential cross section is large where the acceptance is poor, namely in the beam direction. Apart from the almost classical

"two photon" process [3] of fig. 2a we have also considered the four bremsstrahlung like diagrams of fig. 2b [3,4]. Their interference with the two photon process can again be disregarded for the calculation of the total cross section. They only lead to asymmetries between different observed charge combinations, like $e^+\mu^-$ and $e^+\mu^+$. Both classes of processes will be large if one electron is emitted under small angle, i.e. if it stays in the beam pipe. We have neglected the 10 diagrams where the incoming leptons annihilate, which are partially shown in Fig. 2c. They do not lead to a very small momentum transfer anywhere if one or two leptons escape at small angles and with a large missing mass.

Again the corresponding traces have been evaluated and converted into FORTRAN programs with the help of REDUCE. A modification of the standard procedure is however necessary in order to avoid disastrous numerical cancellations at small electron scattering angles. Normally the trace for the electron line (p, p') in Fig. 2a is taken as

$$T^{\mu\nu} = p^\mu p'^\nu + p^\nu p'^\mu + \tfrac{1}{2} g^{\mu\nu} q^2 . \qquad (3.1)$$

For very small angles between p and p', $\vartheta \lesssim \frac{m}{p_0}$, the momentum transfer $q = p - p'$ becomes a multiple of p (and p') up to order $\frac{m^2}{p_0}$. Thus the first two terms in $T^{\mu\nu}$ can be gauged away up to terms of the order $\frac{m^4}{p_0^2}$. At $\sqrt{s}$ = 10 GeV one thus looses at least 16 orders of magnitude. This is easily avoided by adding a multiple of q^μ and q^ν such that the zero-component of the dangerous terms is gauged away:

$$T'^{\mu\nu} = (p^\mu - \lambda q^\mu)(p^\nu - \lambda q^\nu) + \tfrac{1}{2} g^{\mu\nu} q^2 \qquad (3.2)$$

with

$$\lambda = \frac{p_0}{q_0} \quad . \tag{3.3}$$

Taking the beam in the z-direction one finds up to order m^2/s

$$p_z - \lambda q_z = \frac{m^2(\lambda-1) - \lambda\, p\cdot p'}{p_z} + O\left(\frac{m^4}{\sqrt{s}^3}\right) \tag{3.4}$$

which is explicitly very small for $\vartheta \approx 0$. In the REDUCE program $p-\lambda q$ is taken as an independent vector.

Again the calculation of the two photon diagrams (including part of the integration procedure) can be checked by comparison to the Double Equivalent Photon Approximation [3] (DEPA) which holds for the differential cross section integrated over e^+ and e^- directions:

$$\int d\Omega_{e^+} d\Omega_{e^-} \frac{d^8\sigma}{d\Omega_{e^+} d\Omega_{e^-} dE_{e^+} dE_{e^-} d\Omega_{\mu^+}} \approx \frac{N(\omega_1)}{\omega_1} \frac{N(\omega_2)}{\omega_2} \frac{d\sigma^{\gamma\gamma\to\mu\mu}}{d\Omega_{\mu^+}} \tag{3.6}$$

where $\omega_1\,(\omega_2)$ are the energy losses of $e^+(e^-)$ and the photon flux factors $N(\omega)$ are [8] (E = initial, E' = final electron energy)

$$N(\omega) = \frac{\alpha}{\pi}\left[\frac{E^2+E'^2}{E^2}\left(\log\frac{E}{m_e} - \frac{1}{2}\right) + \frac{(E-E')^2}{2E^2}\left(\log\frac{2E'}{E-E'} + 1\right) + \frac{(E+E')^2}{2E^2}\log\frac{2E'}{E+E'}\right] \tag{3.6}$$

and the $\mu\mu$ cross section (for real photons along the beam direction, see Fig. 2a for kinematical notation) is

$$\frac{d\sigma^{\gamma\gamma\to\mu\mu}}{d\Omega_{\mu^+}} = \frac{\alpha^2}{4\omega_1\omega_2} \frac{p_+}{E_- - E_+ p_- \cos\vartheta_{+-}/p_+} \left(\frac{t}{u} + \frac{u}{t}\right) \tag{3.7}$$

with $t = (p_+ - q_1)^2$, $u = (p_- - q_1^2)$. The integrals over $d\Omega_+$ and $d\Omega_-$ are performed with the help of REGINA [7] as mentioned in section 2, and we find agreement between the numerically integrated value and the DEPA result within [+] 5 % for the cross section (3.5).

3.2. Results

In the case of reaction (1.5) an additional difficulty is caused by the experimental requirement that the backgrounds for 2-prong and multiprong events have to be calculated separately. The observability or nonobservability condition for particles 3 and 4 cuts sharply into the phase space and requires a much larger number of integration points. Nevertheless, even in this case we find that the numerical instabilities are well within 10 % for total and 15 % for differential cross sections which is much better than the experimental uncertainties.

In detail, we have calculated the 2-prong background for different charge combinations $\mu^+\mu^-$, μ^+e^-, μ^-e^+ for $\sqrt{s}$ = 4-5 GeV. The results are in

[+] The discrepancies are larger for small muon angles relative to the beam axis, where DEPA is known to be less accurate [3,4].

Table 1. For comparison we also give the (unmeasured) doubly charged combinations μ^+e^+ and μ^-e^- which are the smallest ones. Clearly the biggest contribution comes from the $\mu^+\mu^-$ channel, mainly because in this configuration the missing mass cut does not forbid the large energy of one of the electrons which corresponds to a small virtual photon energy enhancing the cross section like $1/\omega^2$ (see (3.5)). The sum of all neutral channels, which is the real background for the PLUTO experiment is also quoted in Table 1. Note that for comparison with experimental cross sections [2] one has to scale the experimental number down by a ϑ acceptance factor of the order of 0.7.

In the last column of Table 1 we give the results for multiprongs, i.e. $\mu^+\mu^-e^+e^-$, $\mu^+\mu^-e^+$, $\mu^+\mu^-e^-$ ($e^+e^-\mu^\pm$ is very small) seen in the detector. There are no acoplanarity and missing mass cuts in this case which enhances the background quite a lot. It is interesting that the bremsstrahlung part of the cross section (fig. 2b) grows very fast with $\Phi_{AC} \to 0$ and reaches the level of 20 % of the multiprong background, although in the case of 2-prongs it never exceeded 1 %.

In fig. 3 we present $d\sigma/dE_1$ for 2 prong $\mu^+\mu^-$ (long dashed curves) at $\sqrt{s}$ = 5 and 4 GeV, for the total 2 prongs (solid curves) at the same energies and for the multiprong background at 5 GeV (dash-dotted curve). The behaviour of the background is not drastically different from the experimentally observed distributions and after subtraction does not qualitatively change the conclusions of ref. (2).

The symmetric $d\sigma/d\cos\vartheta$ distribution for 2 prong $\mu^+\mu^-$ is given in fig. 4 (solid line). It is very sharply peaked towards $\vartheta = 0$ unlike the distribution from heavy lepton decay [4]. We do not present the asymmetries in this case because the $\mu^+\mu^-$ asymmetry due to the interference terms is very small and the asymmetry $\mu^-e^+ - \mu^+e^-$ and $\mu^-e^+ - \mu^+e^+$, although rather large, is experimentally practically unmeasurable, since the cross sections are smaller than 1 pb.

4. QED-Background at Higher Energies

It is well known [3] that the two photon process cross section increase like $(\log s)^3$ as compared to the $1/s$ decrease of the one photon contribution to lepton pair production. Thus one may wonder whether the heavy lepton signal in the $\mu^+\mu^-$ and μe channels will not be unobservable at PETRA/PEP energies due to this background. The conclusions based on the calculations in ref. (4) were rather pessimistic. Since this is a crucial point for proposed experiments we have investigated this problem again and found that with suitable modifications of the cuts the heavy lepton signal will be clearly observable. Essentially one has to scale the energy cuts and to increase the acceptance.

4.1. Energy scaled cuts

One easily sees from the DEPA approximation (3.5)-(3.7) that the integrations over ω_1 and ω_2 give an increasing factor $(\sim \frac{1}{m_\mu^2} \log \frac{s}{m_\mu^2})$ from the low ω regions, thus leading for $s \to \infty$ to a large two photon cross section. But if one scales the minimal energies of μ^+ and μ^- proportional to $\sqrt{s}$, i.e.

$P_{ex}, P_{min} \sim \sqrt{s}$ and MM $\sim s$, then the $\mu^+\mu^-$ invariant mass has to be of order $\sqrt{s}$ [+)], and both ω_1 and ω_2 have to be of order $\sqrt{s}$. Including one logarithmic factor from (3.6), one expects the QED process to behave like $\log s/s$. This discussion is not quite rigorous, but our results shown in Table 2 agree with this behaviour.

Since the energies of muons from heavy lepton decay are roughly proportional to $\sqrt{s}$, the cross section simply scales down as 1/s even with the scaled cuts, giving 20 pb at $\sqrt{s}$ = 20 GeV, well above the background in Table 2. At this energy there is already a sizeable contribution from the 2-photon production of heavy leptons, which however will be sharply reduced by the above mechanism, and we do not consider it here.

4.2. Detector Acceptance

A large fraction of the 2-photon events has one electron at larger angles. Thus, with a large acceptance for charged particles especially in the forward region, the QED events will be reduced further. Specifically, if charged particles are detected in a range $|\cos\vartheta| \leq .95$, the two prong process (1.5) will decrease further. In Table 2 we show the observed two prong cross section for 4 different sets of experimental cuts. The most important effect clearly comes from the scaling with $\sqrt{s}$, yielding a reduction of a factor of 60, another factor of 2 coming from the acceptance.

+) This is not necessarily true for a small relative angle between μ^+ and μ^-. This case however almost always leads to a large electron emission angle (because of the transverse momentum balance). Thus it is not a two prong event. It can also be excluded by requiring a minimum $\mu^+\mu^-$ angle, which does not affect the heavy lepton cross section.

5. Conclusions

We have presented the calculation of the 4th order QED-background to muon inclusive final channels in e^+e^--annihilation. Our methods of calculation are well suited for "restricted" cross sections, as we

i) explicitly have worked out the integration limits (in laboratory variables) due to the cuts,

ii) can handle the singularities in the angular variables, the type of which is known, easily with REGINA.

The calculation of the differential cross section for process (1.5) was facilitated by a special gauge.

The background at $\sqrt{s}$ = 5 GeV turned out to be around 10 % in the total cross sections and up to 25 % in momentum spectra (especially at small momenta) relative to the observed signal [(2)]. In spite of the large QED-total cross section at PETRA/PEP-energies, we found that the observation of the heavy lepton signal in a PLUTO-like detector is feasible in the 2 prong muon inclusive channel $(\mu^+\mu^-, \mu^\pm e^\mp)$ provided that one uses

i) the energy scaled minimal momentum and missing mass cuts,

ii) a large acceptance for charged particles at small angles, e.g. up to $|\cos\vartheta| \leq 0.95$ in order to reject QED multiprong events.

The detection of another sequential lepton, still heavier than the τ, will be affected somewhat stronger than the τ signal by the energy scaled cuts, the reduction being the same for the same values of $\sqrt{s}/m_{H.L.}$. Of course the expected smaller branching ratio into μ's of a heavier lepton can make its observation rather difficult.

Acknowledgement

We are grateful to all members of PLUTO group, in particular to Drs. V. Blobel, L. Criegee, G. Flügge, G. Knies, H. Meyer and H. Wahl for many helpful discussions. We thank Dr. T. Walsh for a critical reading of the manuscript. One of us (Z.R.) wants to thank Profs. H. Schopper, G. Weber and H. Joos for their warm hospitality extended to him at DESY.

Appendix

A 1 Integration variables

The 7 dimensional integration over the 4-particle phase space is difficult in view of the lengthy matrix elements and their sharp peaking, and we shall be somewhat explicit here. The ideal choice of variables and their order of integration should satisfy two conditions: 1) The integration limits should be explicitly expressible in terms of the cuts and 2) the type of singularity in the dangerous variables should be known. For a cylindrically symmetric detector the first condition suggests spherical coordinates in lab momenta. As we shall see, all experimental cuts listed in sec. 2 are simply expressible in terms of solid angles and energies of the two measured particles. To satisfy the second condition one realizes that the sharpest peaks in cross section correspond to nearby poles of the electron propagators in $e^+e^- \to \mu^+\mu^-\gamma\gamma$ and to nearby poles of the photon propagators in $e^+e^- \to e^+e^-\mu^+\mu^-$. The bremsstrahlungs type of singularity for small γe angles is given in eq. (2.8), the singularity for the second process for small $(e_f^{\pm}, e_i^{\mp})$ angles ϑ_e has the form

$$\frac{d\sigma}{d\vartheta_e} = \frac{\sin\vartheta_e}{(2\sin^2\vartheta_e/2 + \Delta)^2} \times \text{polynomial in } \sin^2\vartheta \qquad (A.1)$$

where

$$\Delta = \frac{2m_e^2}{s}\left(\frac{\sqrt{s}}{2E_e} - 1\right)^2. \qquad (A.2)$$

The energy of the outgoing electron, E_e, actually may depend on ϑ_e, in which case its value at $\vartheta_e = 0$ has to be inserted into (A.2).
We now choose the following sequence of integration:

$$\sigma = \frac{\alpha^4}{8(2\pi)^3}\int \frac{|\vec{p}_1||\vec{p}_2|}{s}\,\frac{|\vec{p}_3|}{|\vec{p}_8|^2 E_4 - E_3\vec{p}_3\cdot\vec{p}_4}\,|T|^2 \qquad (A.3)$$
$$\times\, d\cos\vartheta_1\, dE_1\, dE_2\, d\cos\vartheta_2\, d\varphi_2\, d\cos\vartheta_3\, d\varphi_3 .$$

As mentioned in sec. 2, we always choose the observed μ (identified in the outer detector) as particle number 1 and the second observed particle (μ or e) as particle number 2. Particle 3 has to be the one with the strongest $\cos\vartheta_3$ dependence, i.e. a γ in the process (1.4) and an e^+ or e^- in (1.5). Only the integration limits for particle 1 and 2 are affected by the cuts, whereas the singular integration $d\Omega_3$ is unrestricted.

A 2 Integration limits

The first four cuts (2.2-2.5) give obvious (but not final) limits for our

first four variables:

$$|\cos\vartheta_1| \leq \cos\vartheta_1^{min} \tag{A.4}$$

$$|\cos\vartheta_2| \leq \cos\vartheta_2^{min} \tag{A.5}$$

$$E_1 \geq \sqrt{p_{ex}^2 + m_1^2} = E_1^{min} \tag{A.6}$$

$$E_2 \geq \sqrt{p_{min}^2 + m_2^2} = E_2^{min} \tag{A.7}$$

The acoplanarity cut and the missing mass cut further restrict the ranges: Due to the acoplanarity cut the maximal angle between particle 1 and 2 is given, for each ϑ_1, by

$$\cos\vartheta_{12} \geq -c_m \equiv -\sin\vartheta_1 \sin\vartheta_{2m} \cos\phi_{AC} + \cos\vartheta_1 \cos\vartheta_{2m} \tag{A.8}$$

where

$$\vartheta_{2m} = \begin{cases} \pi - \max\left[\vartheta_2^{min}, \tan^{-1}(\tan\vartheta_1 \cos\phi_{AC})\right] & \text{for } \vartheta_1^{min} \leq \vartheta_1 \leq \pi/2 \\ \max\left[\vartheta_2^{min}, -\tan^{-1}(\tan\vartheta_1 \cos\phi_{AC})\right] & \text{for } \pi/2 \leq \vartheta_1 \leq \pi - \vartheta_1^{min} \end{cases} \tag{A.9}$$

The value (A.8) of c_m determines, via the missing mass cut, the actual upper limits for the two energies:

$$E_1 \leq E_1^{max} = \frac{s + m_1^2 + m_2^2 - MM - 2\sqrt{s}\,E_2^{min}}{2(\sqrt{s} - E_2^{min} - |\vec{p}_2^{\,min}|\,c_m)} \tag{A.10}$$

and, for given E_1, ϑ_1,

$$E_2 \leq E_2^{max} = \frac{s + m_1^2 + m_2^2 - MM - 2\sqrt{s}\,E_1}{2(\sqrt{s} - E_1 - |\vec{p}_1|\,c_m)} . \tag{A.11}$$

The three variables ϑ_1, E_1 and E_2 now define the upper limit for ϑ_{12} again via the missing mass cut:

$$\cos\vartheta_{12} \leq c_x \equiv \min\left[(s + m_1^2 + m_2^2 - 2\sqrt{s}\,(E_1+E_2) + 2E_1E_2 - MM)/2|\vec{p}_1||\vec{p}_2|, 1\right]. \tag{A.12}$$

This formula shows how for a given polar angle of particle one there exists a forbidden cone for particle 2 around the ϑ_1 direction. The limits for ϑ_2 and φ_2 depend purely trigonometrically on the size of this cone and on its intersections with the half planes given by the acoplanarity cut.

Defining

$$a = \cos^2\vartheta_1 + \sin^2\vartheta_1 \cos^2\phi_{AC} \tag{A.13}$$

$$b = c_x \cos\vartheta_1 / a \tag{A.14}$$

$$c = (c_x^2 - \cos^2\phi_{AC} \sin^2\vartheta_1)/a \tag{A.15}$$

we get

$$c_2^{min} \leq \cos\vartheta_2 \leq c_2^{max} \tag{A.16}$$

where

$$c_2^{max} = \begin{cases} b + \sqrt{b^2 - c} & \text{for } \vartheta_1 - \cos^{-1}(c_x) \leq -\vartheta_2^{min} \\ \cos \vartheta_2^{min} & \text{otherwise} \end{cases} \qquad (A.17)$$

$$c_2^{min} = \begin{cases} b - \sqrt{b^2 - c} & \text{for } \vartheta_1 + \cos^{-1}(c_x) \geq \pi + \vartheta_2^{min} \\ -\cos \vartheta_2^{min} & \text{otherwise} \end{cases} \qquad (A.18)$$

Finally, the limits for the φ_2 integration are given by the formula

$$\cos^{-1} c_\varphi \leq \varphi_2 \leq \pi - \phi_{AC} \qquad (A.19)$$

where

$$c_\varphi = \min \left[1, \frac{c_x - \cos \vartheta_1 \cos \vartheta_2}{\sin \vartheta_1 \sin \vartheta_2} \right] \qquad (A.20)$$

(we integrated only over half the domain of φ_2 and, using the symmetry of integrand, multiplied the result by 2).

A 3 The third and fourth particle integration

The remaining integration over Ω_3 has no restriction. However, since the integrand may have as well sharp peaks in Ω_3 as in Ω_4, the latter being not an independent variable, those regions in Ω_3 which correspond to the singular regions in Ω_4 should be integrated over separately. We shall

discuss 3 cases, namely the $\gamma\gamma$ integration with $\mu^+\mu^-$ observed in reaction (1.4), the e^+e^- integration for the same particles observed in reaction (1.5) and the $e\mu$ integration with μe observed in reaction (1.5).

A 3.1 $\gamma\gamma$ Integration

The main contribution here comes from the 8 small cones corresponding to the emission of any of the photons around an electron or a muon direction. We cut out four cones in Ω_3 and perform the angular integral inside these cones with polar coordinates relative to each of the cone axes. This is done with 3 successive applications of REGINA with up to 9 points in one cone. This gives an accuracy better than 0.5 %. The similar cones for Ω_4 give exactly the same contribution due to the $\gamma\gamma$ symmetry, but one has to avoid the configurations when both photons are within the cones. These are however excluded by the acoplanarity cut for sufficiently small cones (empirically we took the cone size around 9^o at 5 GeV). Over the rest of Ω_3 we perform a Monte Carlo integration throwing out the events with a photon in one of the cones. For each muon configuration 25 Monte Carlo points gave a sufficient accuracy.

A 3.2 ee Integration

Here the situation is similar to the previous case except there are only 2 singular cones: One for the final e^- around the direction of the incident e^- and one correspondingly for the e^+. We integrate over both independently and do the rest again by the Monte Carlo method. One should stress here that

the weight function for REGINA as given in (A 1) differs for each set of muon variables, as Δ in (A.2) depends on E_e.

A 3.3 eμ Integration

Since there are no singularities in Ω_μ, this is the simplest case. One integrates over Ω_e treating carefully the small cone around the initial e-direction. The region outside the cone is done by Gaussian integration.

A 4 Symmetrization

The above description is valid only for a well specified experimental trigger, e.g. μ^- in the outer detector, μ^+ in the inner detector, e^+ and e^- unobserved. However, if one wants to calculate the background for e.g. 2 prong double muon inclusive reaction, there must be a symmetric integration of μ^+ and μ^-. It is easy to show using the $\mu^+ \longleftrightarrow \mu^-$ symmetry of the matrix element (in the symmetric integration the interference terms do not contribute) that the domain of the symmetric integration over the variables $\vartheta_1, E_1, E_2, \vartheta_2$ is given by the formula

$$D = D_1 \cup D_2 \tag{A.21}$$

where (see (A 4) - (A 11))

$$D_1 = \{(\vartheta_1, E_1, E_2, \vartheta_2):\ E_1^{min} \le E_1 \le E_1^{max},\ E_2^{min} \le E_2 \le E_1,\ \vartheta_1^{min} \le \vartheta_1 \le \pi - \vartheta_1^{min},\ \vartheta_2^{min} \le \vartheta_2 \le \pi - \vartheta_2^{min}\} \tag{A.22}$$

$$D_2 = \{(\vartheta_1, E_1, E_2, \vartheta_2):\ E_1^{min} \le E_1 \le E_1^{max},\ E_1^{min} \le E_2 \le E_1,\ \cos\vartheta_1^{min} \le |\cos\vartheta_1| \le \cos\vartheta_2^{min},\ \vartheta_1^{min} \le \vartheta_2 \le \pi - \vartheta_1^{min}\} \tag{A.23}$$

and the result must be multiplied by 2. One can also use the $\vartheta_1 \longleftrightarrow \pi - \vartheta_1$ symmetry and integrate always over $\cos\vartheta_1 \ge 0$ which gives another factor of 2.

For $\frac{d\sigma}{dE}$ the symmetry is different because this distribution is a simple sum of $\frac{d\sigma}{dE_{\mu^-}}$ and $\frac{d\sigma}{dE_{\mu^+}}$. In this case one has to integrate over the full region given in A.3 and multiply the result by 2. Note that such a differential cross section after integrating over E will not give the total cross section times the multiplicity. This corresponds to the fact that the events with both muons identified in outer detector will be counted twice on the experimental histogram.

In the case of asymmetry calculation one has to calculate $\frac{d\sigma}{d\cos\vartheta_{\mu^-}}$ and $\frac{d\sigma}{d\cos\vartheta_{\mu^+}}$ independently. The interference terms do not vanish then and there is no symmetry in $\cos\vartheta$.

Table 1

$\sqrt{s}$ [GeV]	$\sigma_{\mu\mu\gamma\gamma}$ [pb]	2 prongs [pb]				multiprongs [pb]
		$\mu^+\mu^-$	$\mu^-e^+ + \mu^+e^-$	$\mu^-e^- + \mu^+e^+$	Total(neutral)	
4.0	7.0	4.8	0.39	0.12	12.2	14.9
4.5	6.7	9.7	0.72	0.20	17.1	16.6
5.0	6.6	15.0	1.14	0.32	22.7	16.7

Total background cross sections for PLUTO from processes (1.4) and different configurations of (1.5) in the energy range 4-5 GeV.

Table 2

Cuts			$\sigma_{2pr.}^{\mu^+\mu^-(e^+e^-)}$	$\sigma_{\mu\mu\gamma\gamma}$
p_{ex} [GeV]	p_{min} [GeV]	$\cos\vartheta_2^{min}$	[pb]	[pb]
1.0	0.25	0.87	85	1.2
4.0	1.0	0.87	1.3	not calc.
4.0	1.0	0.91	0.9	"
4.0	1.0	0.95	0.6	"

Total cross sections of the processes (1.4) and (1.5) at $\sqrt{s}$ = 20 GeV for different experimental cuts. The cuts which are not explicitely mentioned in the table remain unchanged (see text). The heavy lepton signal for the cuts in the last row is expected to be about 20 pb.

References

1. M.L. Perl et al., Phys. Rev. Lett. 35 (1975) 1489,
   M.L. Perl et al., Phys. Lett. 63B (1976) 466,
   H. Cavalli-Sforza et al., Phys. Rev. Lett. 36 (1976) 558,
   G.J. Feldman et al., Phys. Rev. Lett. 38 (1977) 117.

2. J. Burmester et al., DESY 77/24 (1977); DESY 77/25 (1977),
   H. Meyer, DESY 77/19 (1977),
   G. Flügge, DESY 77/35 (1977).

3. See e.g. S.J. Brodsky, T. Kinoshita, H. Terazawa, Phys. Rev. Lett. 25 (1970) 972; Phys. Rev. D4 (1971) 1532; H. Terazawa, Rev. Mod. Phys. 45 (1973) 615; G. Grammer, Jr., T. Kinoshita, Nucl. Phys. B80 (1974) 461 and references therein.

4. R. Bhattacharya, J. Smith, G. Grammer, Jr., Stony Brook preprint ITP-SB-77-3,
   J. Smith, J.A.M. Vermaseren, G. Grammer, Jr., Stony Brook preprint ITP-SB-77-5.

5. REDUCE 2, Users Manual, A.C. Hearn, Stanford Memo ATM - 133, 1970

6. D.R. Yennie, S.C. Frautschi, H. Suura, Ann. Phys. 13 (1961) 379.

7. See the forthcoming description of REGINA (by F. Gutbrod) in DESY-R-INFO (1977).

8. R.H. Dalitz, D.R. Yennie, Phys. Rev. 105 (1957) 1598.

Figure Captions

Fig. 1. The diagrams contributing to the process $e^+e^- \to \mu^+\mu^-\gamma\gamma$ in lowest order.

a) - d) "single radiation" diagrams;

e) - g) electron "double radiation" diagrams;

h) - j) muon "double radiation" diagrams.

Fig. 2. The diagrams contributing to the process $e^+e^- \to e^+e^-\mu^+\mu^-$ in lowest order.

a) two photon type

b) bremsstrahlung type

c) annihilation type (neglected).

Fig. 3. The energy distribution $\frac{d\sigma}{dE}$ of muons in $e^+e^- \to \mu^+\mu^-\gamma\gamma$ at 4 and 5 GeV (short dashed lines), in $e^+e^- \to e^+e^-\mu^+\mu^-$ at 4 and 5 GeV (long dashed lines), total 2 prong at 4 and 5 GeV (solid lines) and multiprong at 5 GeV (dash-dotted line).

Fig. 4. The angular distribution of muons, $\frac{d\sigma}{d\cos\vartheta}$ for the symmetric and asymmetric case in $e^+e^- \to \mu^+\mu^-\gamma\gamma$ and for 2 prong symmetric case in $e^+e^- \to e^+e^-\mu^+\mu^-$. For the definitions see Secs. 2.4 and 3.2.

Fig. 5. The $\mu\mu$ asymmetry (2.8) in $e^+e^- \to \mu^+\mu^-\gamma\gamma$.

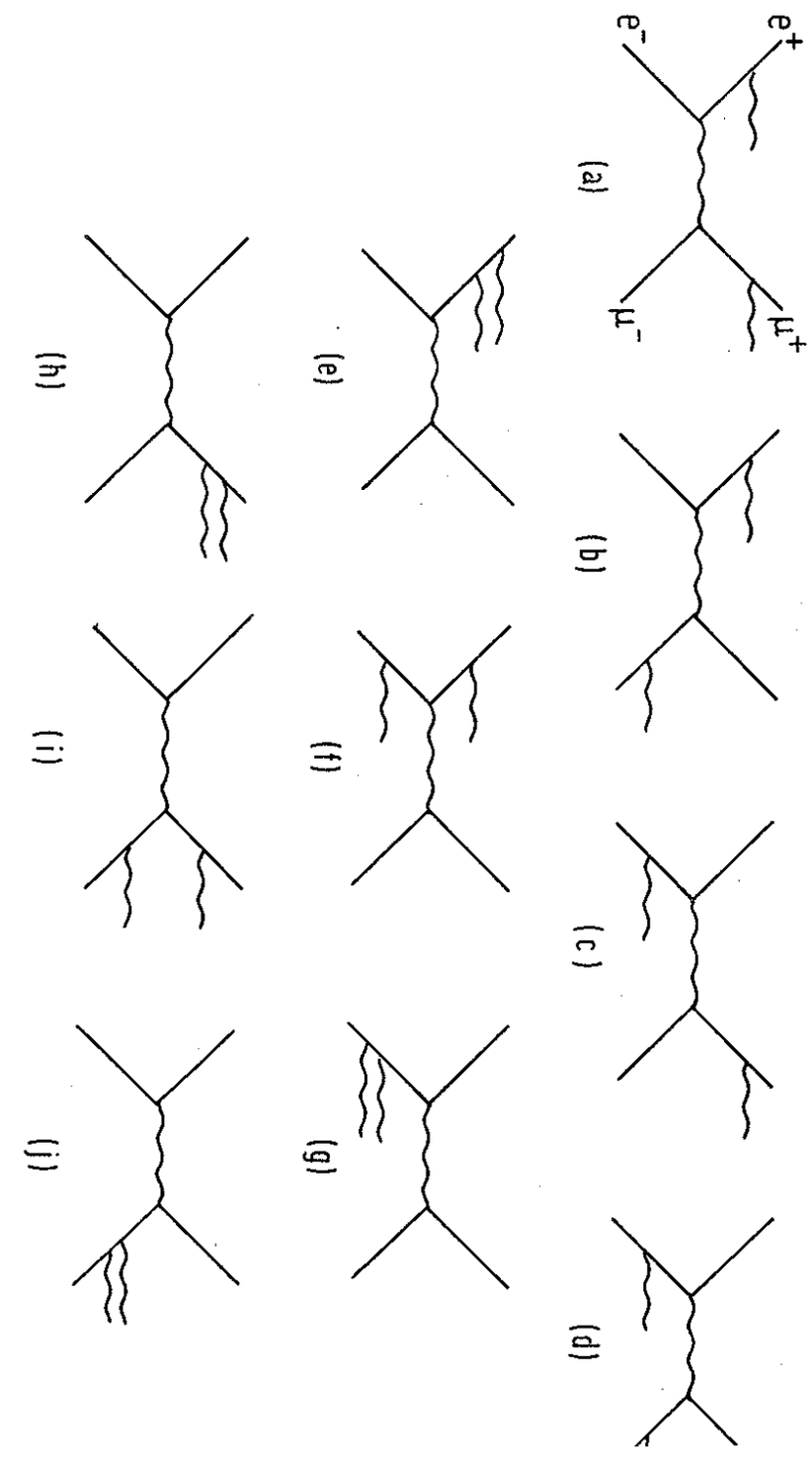

Fig. 1

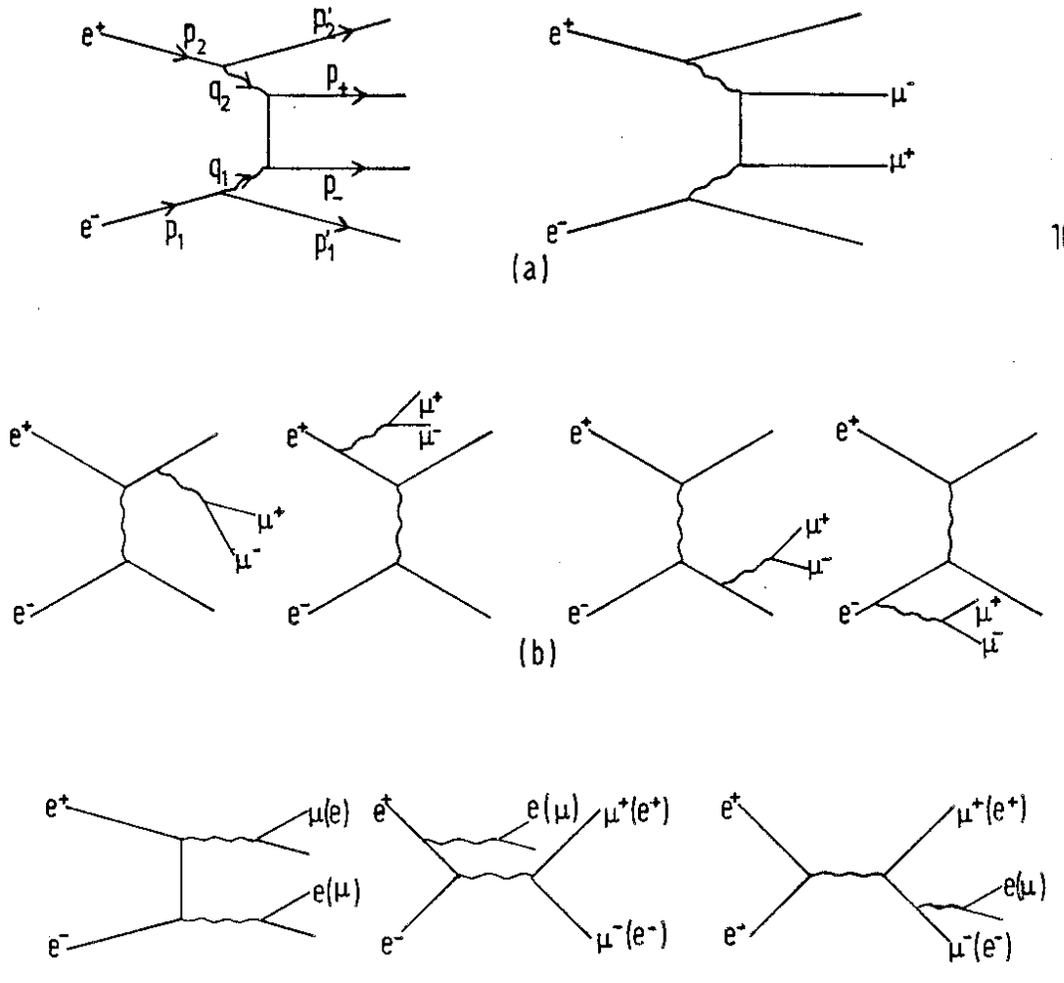
e+
p2
p'2
q2
p+
q1
p-
e-
p1
p'1
(a)
μ-
μ+
(b)
μ(e)
e(μ)
μ+(e+)
μ-(e-)
(c)

Fig. 2

Fig. 3

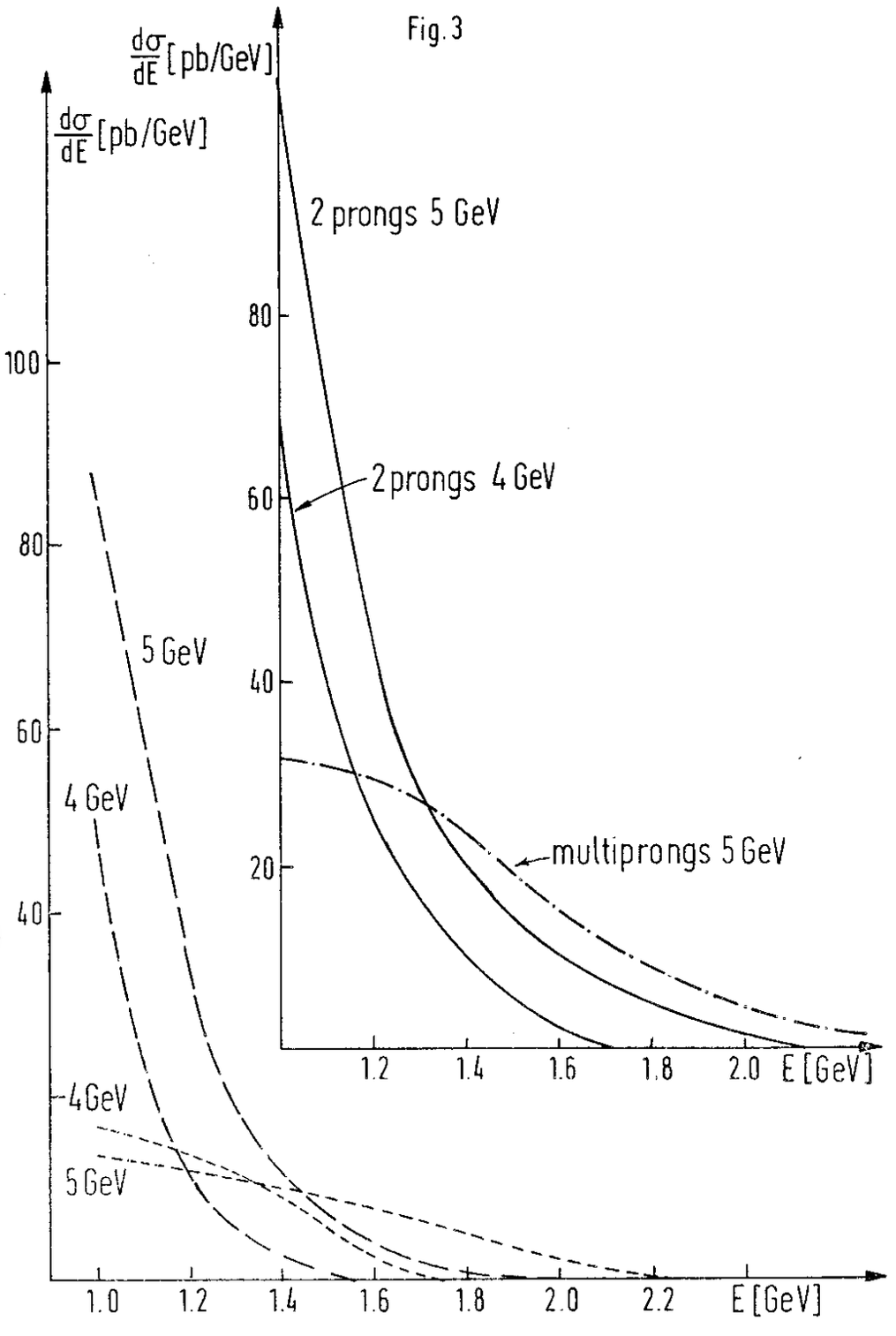
dσ/dE [pb/GeV]
2 prongs 5 GeV
2 prongs 4 GeV
multiprongs 5 GeV
5 GeV
4 GeV
4 GeV
5 GeV
E [GeV]
E [GeV]

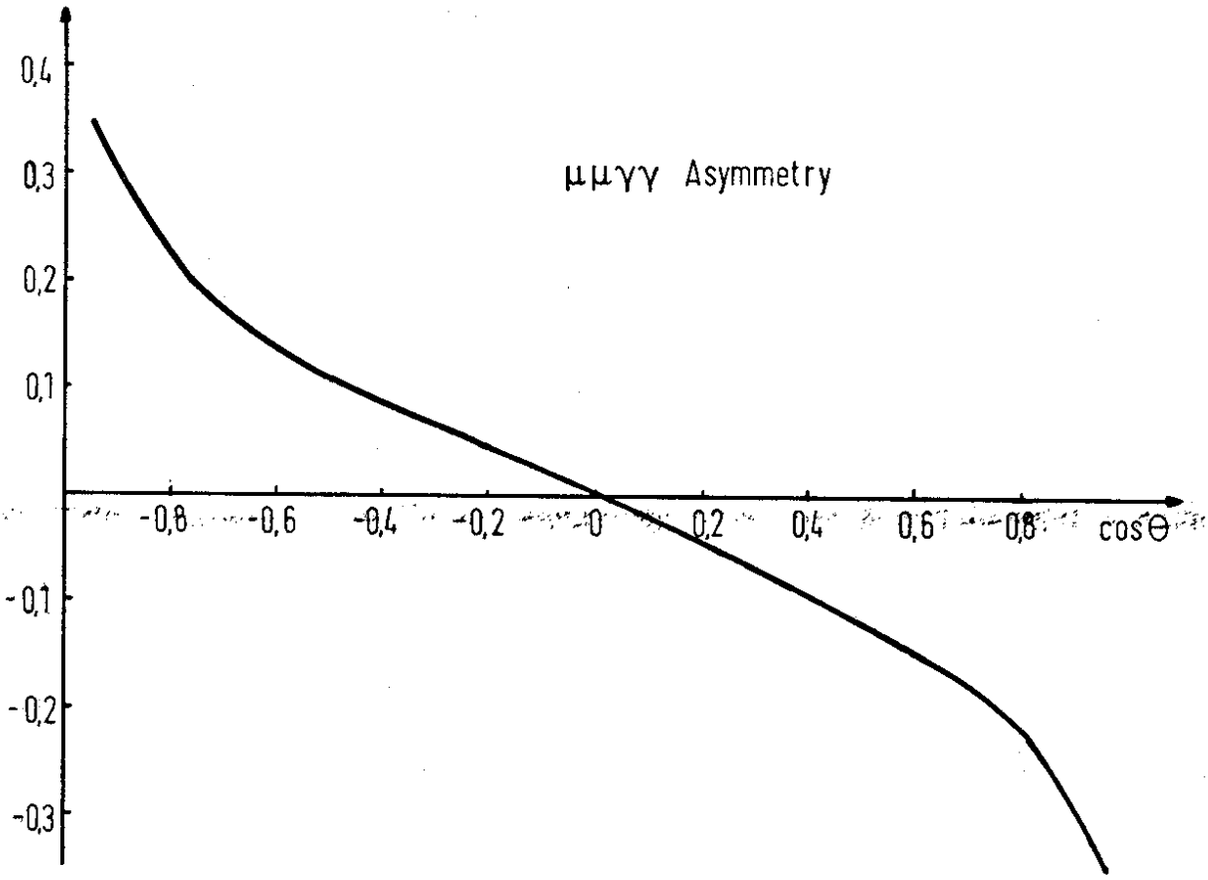
μμγγ Asymmetry
0,4
0,3
0,2
0,1
-0,1
-0,2
-0,3
-0,8
-0,6
-0,4
-0,2
-0
0,2
0,4
0,6
0,8
cosΘ

Fig. 5

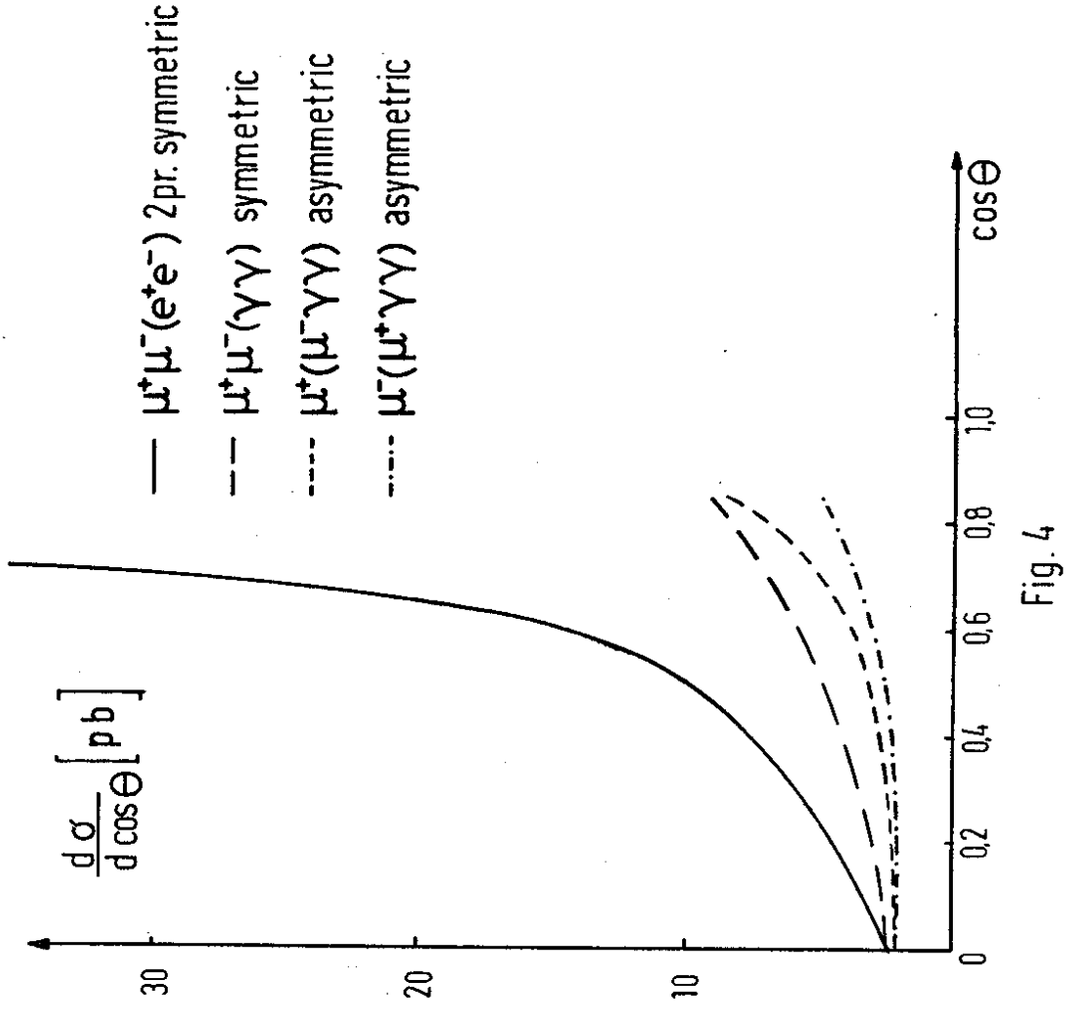
— μ⁺μ⁻(e⁺e⁻) 2pr. symmetric
– – μ⁺μ⁻(γγ) symmetric
– – – μ⁺(μ⁻γγ) asymmetric
– · – · μ⁻(μ⁺γγ) asymmetric
dσ/d cosΘ [pb]
30
20
10
0
0,2
0,4
0,6
0,8
1,0
cosΘ

Fig. 4